

UNSTEADY EFFECTS OF THE SEPERATED FLOW AT THE TAIL SECTION OF A HELICOPTER FUSELAGE

F. Vogel, C. Breitsamter, N. A. Adams
Institute of Aerodynamics, Technische Universität München
Boltzmannstr. 15, 85748 Garching, Germany
Tel.: +49 89 289 16171, email: Florian.Vogel@aer.mw.tum.de

Abstract

The flow around a helicopter fuselage was investigated experimentally. For this purpose a scaled wind-tunnel model was instrumented with steady and unsteady pressure probes at the lower part of the fuselage tail section. The flow field in the wake area of the helicopter was measured with a Stereo-PIV system. A strong positive pressure gradient followed by stagnation at the lower tail section of the fuselage defines the flow separation. The pressure distribution for the base line case show some indications of vortex generation at the tail, which develops downstream and can also be detected by the flow field measurements. The influence of the support strut of the wind tunnel model was demonstrated by two model mount variations. The vortex strength is reduced by the disturbing effect of the support strut. A first estimation of the position of boundary layer transition was made. The unsteady effects of the flow separation at the lower tail section of the fuselage were investigated.

NOMENCLATURE

c_p	=	dimensionless pressure coefficient
$c'_{p\text{ rms}}$	=	root mean square of pressure fluctuation
A_{ref}	=	reference area (cross section area of the fuselage)
f	=	frequency
k	=	reduced frequency
l_{ref}	=	reference length ($l_{\text{ref}} = \sqrt{A_{\text{ref}}}$)
U_{∞}	=	free stream velocity
u, v, w	=	axial, lateral, vertical velocity component
u', v', w'	=	axial, lateral, vertical velocity fluctuation component
Re	=	Reynolds number
α	=	angle of attack
β	=	angle of sideslip
φ	=	angle of vertical surface slices
ω	=	axial vorticity component

1. INTRODUCTION

The aerodynamic design of the helicopter fuselage is an important issue in the development process of a rotorcraft. The objective is not only to reduce aerodynamic drag in fast forward flight, but also to reduce or to prevent dynamic effects of the flow, which could lead to undesirable structural dynamic loads or material fatigue of fuselage components.

The design of the fuselage shape varies with the application range of a helicopter. For a light-weight transport-helicopter configuration, such as investigated in this case, the accessibility from the rear and a large cargo volume in the fuselage are of major interest. For this reason, the tail section of the fuselage is strongly curved. This specific shape of the tail leads to a complex behaviour of the flow, with cross flow separation and vortex rollup of the separated boundary layer [1], [2].

Several investigations on a helicopter fuselage have been conducted [3], [4]. Force and pressure measurements were made, to provide a database for validation of different numerical methods. The focus of these investigations was the prediction of the aerodynamic forces, in particular the drag. The fuselage geometry for these investigations was of streamlined shape, on which rarely flow separation occurs. Numerical investigations on the same fuselage, such as the one which is used here, were made to compare different codes and turbulence models [5], [6]. It was shown that the complex separation structures at the tail section are hardly predictable, even by higher-order turbulence models. The former studies on this fuselage shape showed that a more detailed understanding of the flow is necessary not only to make progress in modelling such flow phenomena numerically but also to find out more about the interaction of the wake with components of the helicopter.

This work aims at improving the understanding of the flow physics for such geometries. For this purpose, an analysis of the flow separation is based on the surface pressures in the lower part of the

fuselage tail section. The influence of the support strut on the flow around the lower part of the tail section of the fuselage is also investigated.

2. EXPERIMENTAL SETUP

2.1. Wind-tunnel facility

All experiments have been performed in the low-speed wind-tunnel facility of the Institute of Aerodynamics at the Technische Universität München. The wind-tunnel has an open test section with a length of 4.8 m. The cross section at the inlet is of 2.4 m width and 1.8 m height. The turbulence intensity of the free stream is for axial, lateral and vertical velocity components smaller than 0.4%. For the open test section a maximum free stream velocity of 65 m/s can be achieved.

2.2. Wind-tunnel model

For the experiments a scaled helicopter model was used. The model consists of the helicopter fuselage, the tailboom, the empennage, a removable rotorhub and the model mount (Fig. 1). The shape of the fuselage is that of a light-weight helicopter configuration. To simplify the geometry, the landing gear is removed and the engine inlets and outlets are closed. At the end of the tailboom a profiled tail rotor mount is connected. The empennage system consists of a horizontal stabilizer which provides the helicopter with stability in pitch in cruise. Endplates at both sides of the horizontal stabilizer for a stabilizing moment in yaw are used. The support strut is of cylindrical shape with a diameter $d/l_{ref}=0.19$.

Two ways for mounting the model in the wind tunnel test section are possible. The standard variant is from the lower side of the fuselage (Fig. 1a). To investigate the influence of the support strut on the flow around the lower tail section of the fuselage the model can be turned up side down (Fig. 1b).

For the bottom-side model mount, there is a mechanism for automatic variation of the angle of attack in a range of $\alpha = \pm 40^\circ$. The axis of rotation is placed close to the connection of the support strut to the fuselage. A hinge in the support strut allows for the adjustment of the angle of attack for the mount on the upper side of the fuselage. The support strut is connected to a rotating disc on the test section floor, which allows the variation of sideslip in a range of $\beta = \pm 180^\circ$.

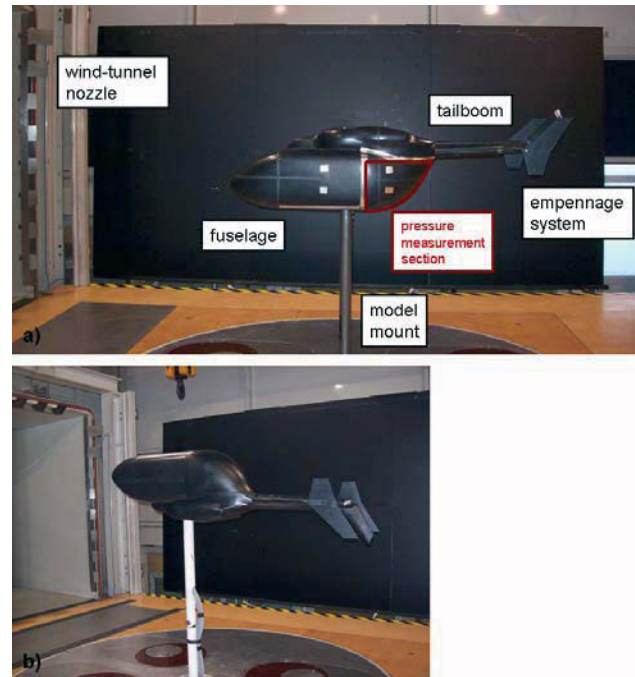


Fig. 1: Wind-tunnel model

2.3. Measurement techniques

The experiments include different types of measurement techniques. Surface pressures were measured in the lower tail section by use of steady and unsteady pressure tabs. The wake of the fuselage was investigated by velocity measurement with a Stereo-PIV system.

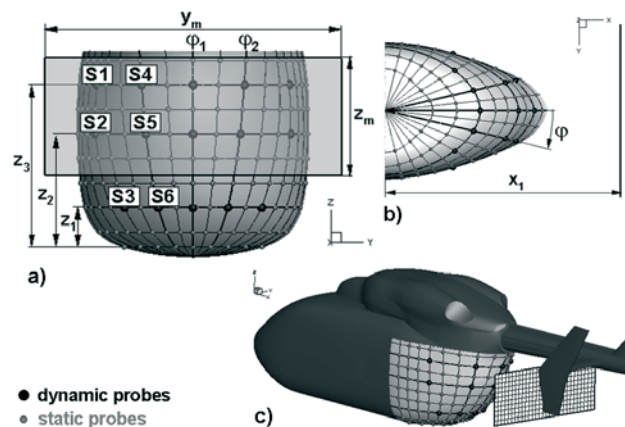


Fig. 2: Experimental setup: Distribution of steady and unsteady pressure tabs, PIV measurement plane

2.3.1. Steady pressure measurements

The wind-tunnel model is equipped with 128 wall tabs to measure the mean surface pressures. These sensor locations are arranged on the lower part of the fuselage tail according to a distribution presented in Fig. 2. The tab diameter is $d_T=0.3$ mm.

The wall tabs are connected to a multiport pressure measurement system, which measures the 128 ports successively. A sampling rate of 100 Hz was used and the pressure was averaged over a time of $t_m=5$ s. The full scale range of the system is FS=17 kPa with an accuracy of $\pm 0.15\%$ FS.

2.3.2. Unsteady pressure measurements

For the unsteady pressure measurements the tail section of the fuselage is instrumented with 15 unsteady pressure transducers according to the positions presented in Fig. 2. The transducers are connected to the same type of wall tabs like the steady pressure measurement system. The output voltage of the sensors is amplified and low-pass filtered at 1000 Hz. The signal was sampled with 3000 Hz over a time interval of 30 sec. The full scale range of the sensor is FS=2.5 kPa with an accuracy of $\pm 0.25\%$ FS.

2.3.3. Velocity field measurements

For the velocity field measurements a Stereo-PIV system was used. The laser light sheet was placed perpendicular to the free stream flow. The cameras are positioned from one side outside the test section. The incidence angle of the cameras on the laser sheet is of $\psi=\pm 20^\circ$, the observation distance is $z_0=2.0$ m. A pulse delay of 15 μ s was chosen between the two frames of one recording and the velocity field was averaged over 100 recordings.

3. RESULTS AND DISCUSSION

Several different cases were treated in this paper. The model mount was connected to the wind-tunnel model from the lower side of the fuselage and from the upper side. For both configurations a Reynolds number investigation was made. Finally an angle of attack variation was conducted.

3.1. Baseline configuration

The baseline configuration represents the wind-tunnel model at angle of attack and sideslip $\alpha=\beta=0^\circ$. The Reynolds number for this case was $Re=6.4 \times 10^5$ ($U_\infty=40$ m/s).

The flow phenomena occurring around the lower tail section of the fuselage of this helicopter type are not well established. Earlier investigations detecting a strong vortex pair in the wake. Their origin is expected somewhere on the lower fuselage tail under the tailboom connection.

3.1.1. Mean flow

The standard model mount for such helicopter fuselage models in the wind tunnel test section is

with a support strut connected on the bottom side of the fuselage. For the investigation of the flow around the lower tail section, the influence of the strut wake is of considerable importance. Therefore the baseline case is also investigated with the upper mount variant, where less influence of the support strut on the flow around the lower tail section is expected.

In Fig. 3, the pressure distribution on the tail section of the fuselage is shown for both mount cases. The measured pressures were averaged in time and mapped onto the fuselage surface.

The comparison of the upper and lower mount for the support strut shows significant differences in the distribution of the surface pressure on the fuselage tail. A strong positive pressure gradient can be detected for both cases on the sidewalls. For the upper mount the pressure gradient form a closed line around the lower tail section. The lower mount case has this strong pressure increase on both sidewalls, but a smooth gradient at the lower middle part, where the wake of the support strut is expected. The narrow band of a pressure rise right below the tailboom at the centreline is missing for the lower mount case. Two elliptical zones with lower pressure can be seen in the area of flow separation for the upper mount case. These areas give an indication of a vortex pair with its origin at that location.

The generation process of these vortices can be explained by a type of crossflow separation on the lower tail section. The flow along the fuselage sidewalls separates due to a strong positive pressure gradient. The flow along the fuselage floor remains attached and merges with the separated part in a rollup process below the tailboom.

In Fig. 4, the pressure distributions along the z-axis for two slices of φ are shown. The comparison of the pressure gradients along the φ_1 -slice exhibits more clearly the differences between the two model mount versions.

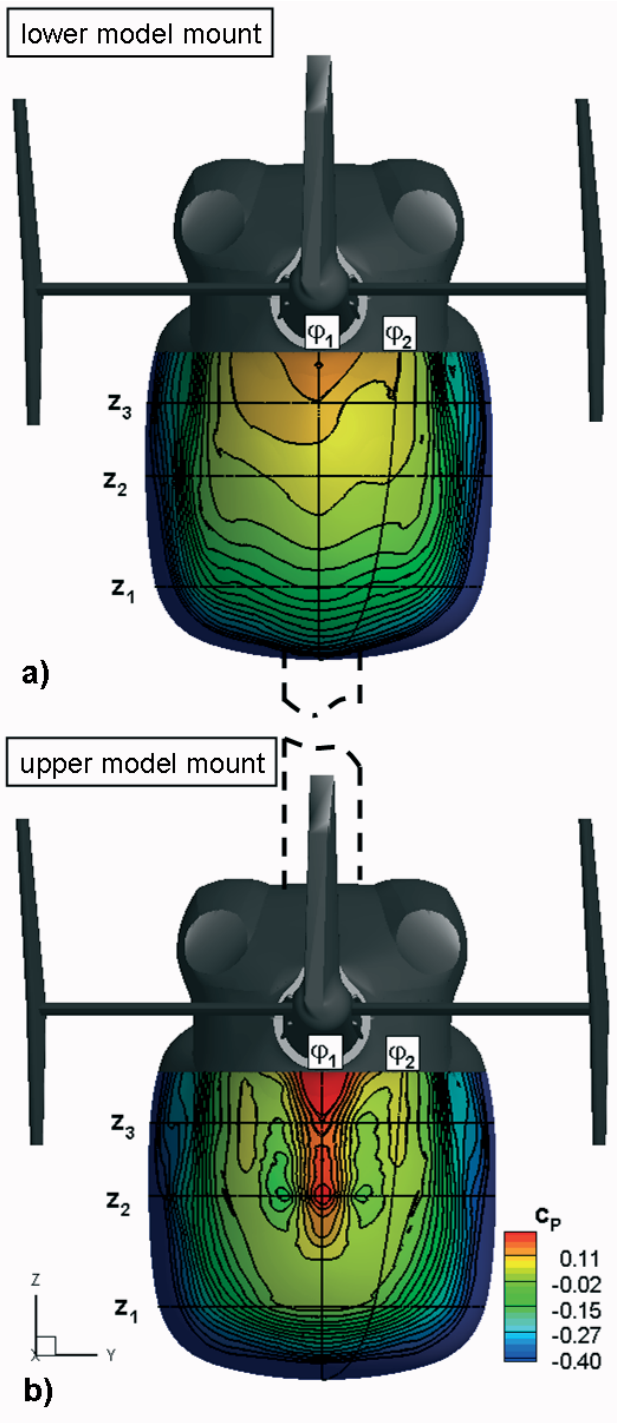


Fig. 3: Pressure distribution at fuselage tail section - with upper and lower wind tunnel mount

The undisturbed flow around the tail of the upper mount case has a strong pressure increase interrupted by a short stagnation region at $z/l_{ref}=0.1$ and a local minimum at $z/l_{ref}=0.5$. The pressure level in the wake of the strut is higher compared to the upper mount case at $z/l_{ref}<0$ and a smooth positive pressure gradient can be noticed upwards. For the φ_2 -slices the pressure characteristics for both mount variants are pretty similar, which means the strut wake has less influence on the flow of the lower

mount case.

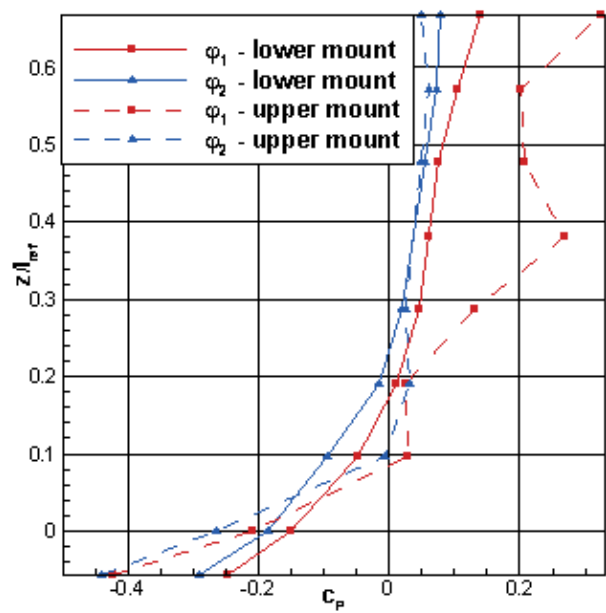


Fig. 4: Pressure distributions for two slices $\varphi_1=0^\circ$, $\varphi_2=13^\circ$

The pressure gradients along two horizontal cuts can be seen in Fig. 5. The positive gradients along the sidewalls at $|\varphi|>30^\circ$ are slightly larger for the lower mount case at z_1 . At z_3 a precise difference between the two cases can be detected in the area around the symmetry plane, where the vortex generation for the upper mount case is located.

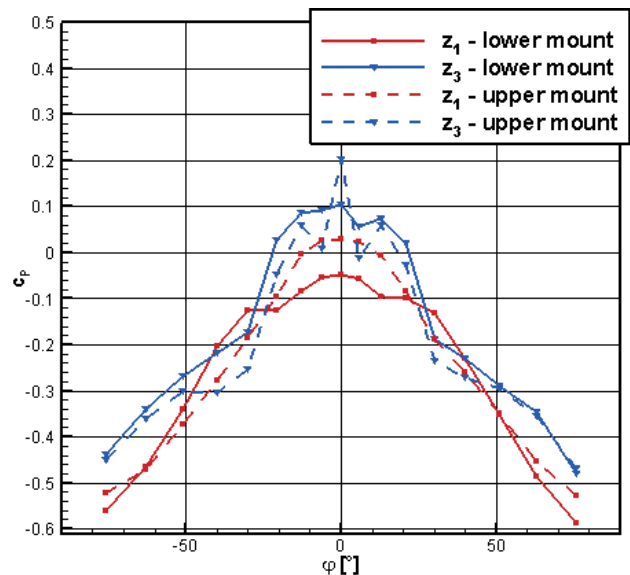


Fig. 5: Pressure distributions for three horizontal slices $z_1/l_{ref}=0.095$, $z_3/l_{ref}=0.57$

3.1.2. Velocity field

The velocity field of the wake was measured at a distance of $x_1=1.55 \cdot l_{ref}$ behind the model (Fig. 2b,c).

The position of the plane is just below the tailboom. In Fig. 6, the axial velocity component with streamlines is shown. A slight asymmetry with respect to the centerline can be seen for both mount variations. The upstream influence of the end plates of the empennage leads to this effect. These endplates are mounted with an angle to the right on the horizontal stabilizers to deflect the flow and produce a side force.

As the pressure distributions on the fuselage tail already indicates, there is also a strong difference in the velocity fields of the two mount variants. The case with the lower mounted support strut has a larger area of low velocity, which defines the fuselage wake. Without any disturbances of the strut the flow stays attached longer, which leads to a smaller wake area (Fig. 6b). For both cases the streamlines show an upstream effect around the centerline. A vortex pair can be detected for the upper mount case. The vortices are counter rotating and the streamlines describe a strong distortion of the flow coming from the lower side. The wake influenced by the lower strut does not clearly show this vortex development, but also indicates a vortex pair by strongly curved streamlines in the upper section of the measurement plane.

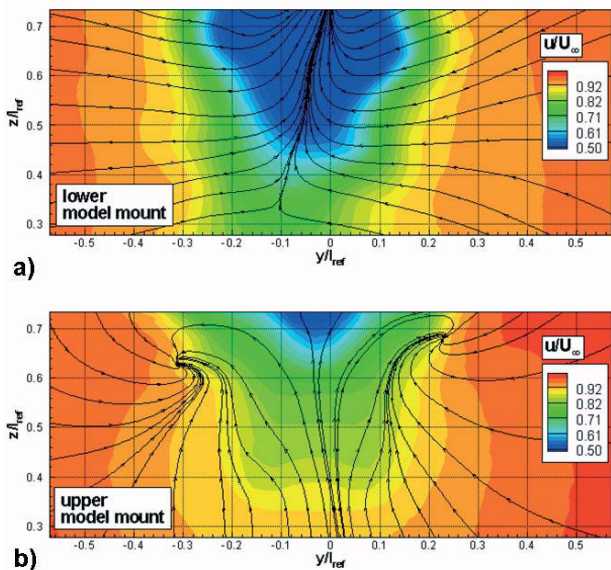


Fig. 6: Axial velocity field at $x/l_{ref}=4.2$

In Fig. 7, the axial vorticity ω for both mount variations is displayed. Again, the influence of the strut can be seen clearly. Two spots of high vorticity indicate the vortices for the upper mount case. The sustained and bended shapes of these two spots are reflecting the strong distortion of the streamlines in Fig. 6b). Between this primary vortex pair a second pair of vortices can be seen, smaller in size and counter rotating. For the upper mount case the vorticity field is more diffusive and the primary vortex pair is much weaker there.

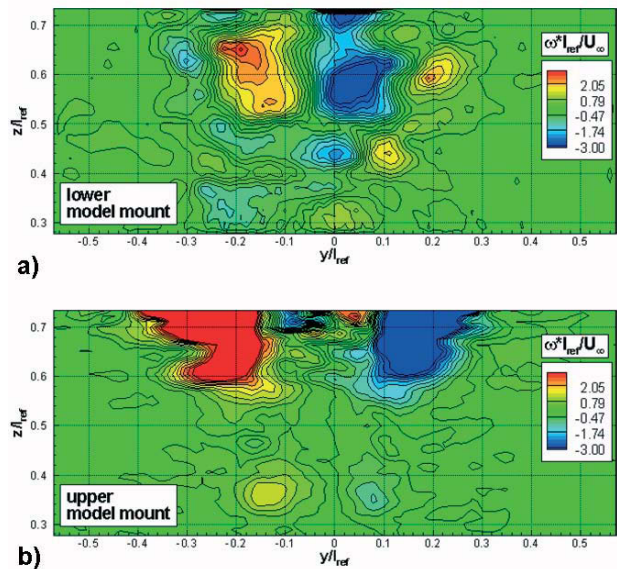


Fig. 7: Axial vorticity distribution at $x/l_{ref}=4.2$

3.1.3. Dynamic effects

The root mean square of the pressure fluctuations measured with the unsteady pressure sensors on the model surface can be seen in Fig. 8 for three horizontal slices. The two mount variants are plotted. Considering the z_1 -slice, a strong rise of the surface pressure fluctuations for the lower mount case can be noticed. The two strong peaks of the c_{Prms} on both sides of the centerline represents the influence of the vortex shedding of the support strut on the surface pressure of the lower tail section.

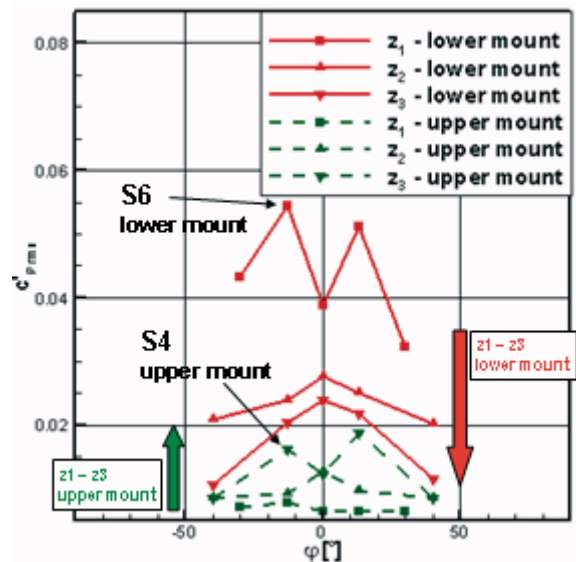


Fig. 8: Root mean square of the pressure coefficient at three horizontal slices $z_1/l_{ref}=0.095$, $z_2/l_{ref}=0.38$, $z_3/l_{ref}=0.57$ for lower and upper mount variations

The intensity of the turbulent fluctuations in the strut wake decrease along the tail upstream, as it can be seen by the z_2 - and z_3 -slice. For the upper mount case at z_1 the c_{Prms} has a minimum level and is

continuously rising from z_1 to z_3 . The maximum peaks for the lower mount case can be discovered on the z_3 -slice on the left and right side of the centerline. In this area the two low pressure spots, where the vortex generation takes place, are located (Fig. 3b)). The fluctuations on the z_3 -slice for both cases showing in the sidewalls $|\phi| > 50^\circ$ a similar characteristics, caused by lower impact of the strut wake.

The power spectral density for the surface pressure fluctuations at one side of the tail for the upper and lower mount case are displayed in Fig. 9. The location of each sensor point (S1-S6) can be found in Fig. 2a).

For each mount case the points with maximum fluctuations (Fig. 8) are considered first. The sensor point S6 has the maximum C_{Prms} for the lower mount variant. The spectra has an amplitude enhancement at $k=0.8$, which corresponds to the frequency determined with the strouhal number of a cylinder. For the upper mount case the amplitude level is in general lower and the enhancement is nonexistent. Sensor point S4 represents the maximum C_{Prms} for the upper mount case. The power spectral density doesn't give any indications of dominant frequencies.

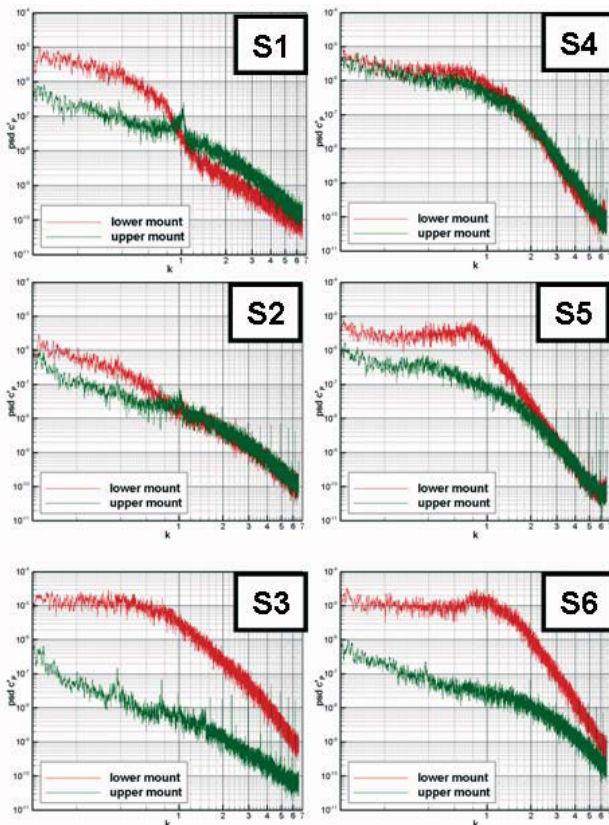


Fig. 9: Power spectral densities of surface pressure fluctuation coefficient on fuselage tail over reduced frequency $k = (f \cdot l_{ref}) / U_\infty$

The vortex pair produces a significant amount of

turbulence. In Fig. 10, the field of the axial, lateral and vertical velocity fluctuation is displayed. All three velocity distributions are showing three spots of higher turbulence. The two outer spots are located close to the cores of the primary vortex pair. Also an area of higher fluctuations is located between the primary vortex pair, which belongs to the second vortex pair. The maximum perturbation can be detected for the lateral velocity component. An interaction of these fluctuations with the tailboom is possible and should be investigated in future.

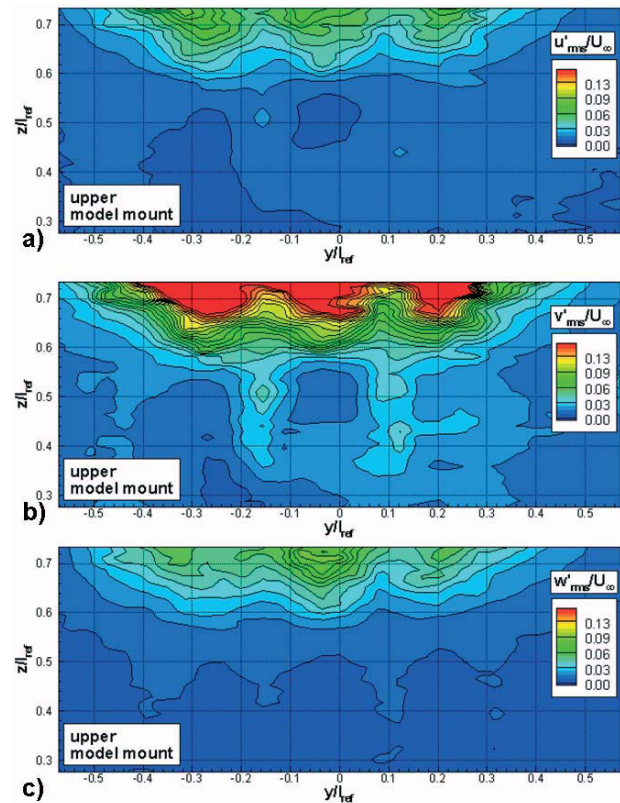


Fig. 10: Root mean square of the three velocity fluctuation components u' , v' , w' at $Re_3 = 6.4 \times 10^5$

3.2. Reynolds number influence

The flow behaviour in the tail section of the fuselage depends on the development of the boundary layer around the fuselage. Especially the position of the transition between laminar and turbulent boundary layer is important for the velocity profile and the thickness of the boundary layer and thus also for the position of the flow separation downstream on the fuselage tail.

3.2.1. Transition

To investigate the influence of the Reynolds number on the transition at the model, a microphone probe was used. The probe consists of a pitot tube connected to a microphone. The recorded audio

signal is amplified and given out to a headphone. The transition point can be detected qualitatively by moving the probe on the model surface in flow direction, till strong noises can be observed. On 14 points around the fuselage the transition points were qualitatively defined and interpolated with a spline-function on the model surface.

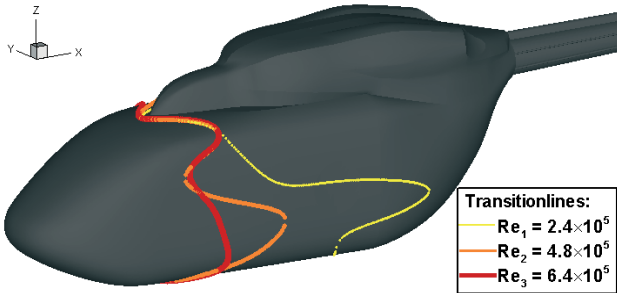


Fig. 11: Transition location for three Reynolds numbers

The transition was investigated for three Reynolds numbers $Re_1=2.4 \times 10^5$, $Re_2=4.8 \times 10^5$ and $Re_3=6.4 \times 10^5$. Therefore the model was mounted from the lower side on the support strut.

The transition position on the upper part of the fuselage does not change visibly for the three different Reynolds numbers. The upstream influence of the engine canopy initiates the transition process. On the sidewalls of the fuselage the largest differences between the three cases can be seen. Especially for the Re_1 -case a significant transition delay is detected.

3.2.2. Surface pressure

In Fig. 12 the surface pressure distribution of the upper and lower mount for different Reynolds numbers is plotted. The pressure distribution for Re_1 shows an asymmetry in the area of low pressure with respect to the centerline. This asymmetry can be found for both mount variations and is getting weaker with increasing Reynolds number. For the upper mount case, the pressure level in the separation area decreases with increasing Reynolds number and the two spots of low pressure produced by the vortex pair are growing. Even though these Reynolds number influences are detected in the upper part of the tail, there is no significant change in the pressure distribution at the lower section, where the transition line for Re_1 on the same height is differing quite much from the two higher Reynolds numbers (Fig. 11).

In Fig. 13, the $c_{P_{rms}}$ characteristic along three z-slices for different Reynolds numbers is displayed. Just the upper mount case is investigated here, to isolate the dominant influences of the strut wake on the unsteady flow behaviour around the fuselage tail.

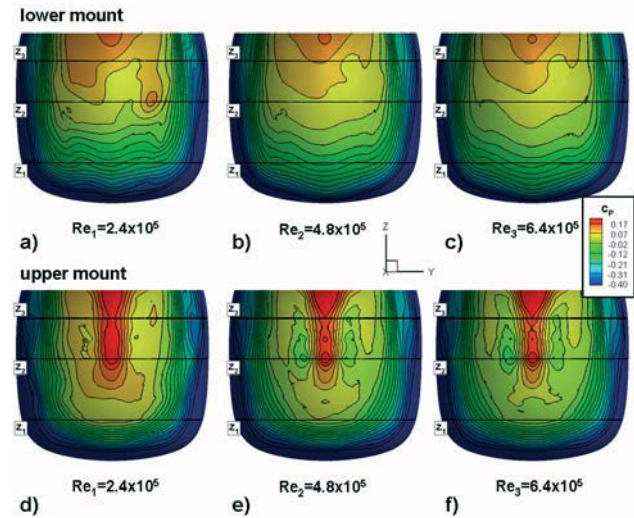


Fig. 12: Surface pressure distribution on the fuselage tail section for three different Reynolds numbers

In general the flow with the lowest Reynolds number represents the strongest dynamic load. The distribution of the $c_{P_{rms}}$ for Re_1 shows two peaks at $\varphi=0^\circ$ for z_2 and z_3 , these peaks are lying in the narrow band of higher pressure (Fig. 12e). The peak at z_2 is getting smaller for Re_2 and Re_3 . For z_3 the maximum in the middle disappears and two smaller peaks at each side of the center line come up. The two peaks are crossing the generation point of the vortex pair.

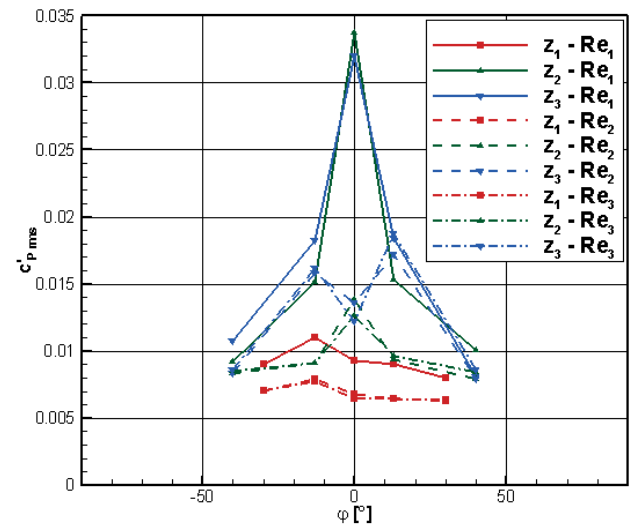


Fig. 13: Root mean square of the pressure coefficient at three horizontal slices $z_1/l_{ref}=0.095$, $z_2/l_{ref}=0.38$, $z_3/l_{ref}=0.57$ for three Reynolds numbers (upper mount case)

3.3. Variation of angle of attack

The helicopter is going through different flight conditions during an operation. The flow separation and the generation of vortices at the fuselage tail

change due to that influence.

In Fig. 14 the surface pressure for an angle of attack range of $\alpha=\pm 10^\circ$ are investigated. With changing angle of attack in negative direction the narrow band of high pressure at the centerline is contracted and split up by the two low pressure spots of the vortex pair. The pressure in the cores drops as the pressure level in the separation zone does.

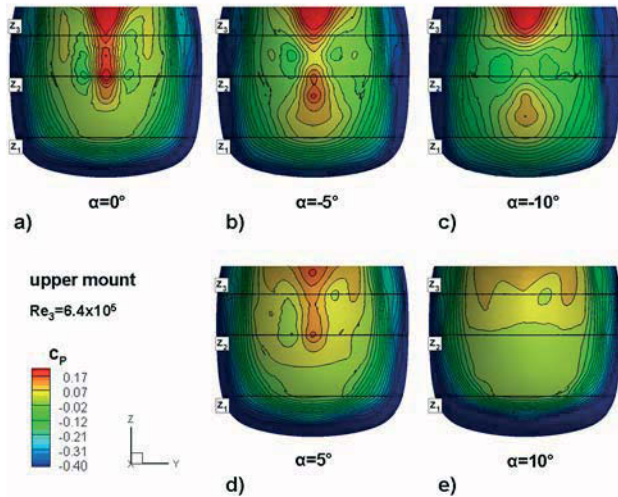


Fig. 14: Surface pressure distribution on the fuselage tail section for angle of attack variation $\alpha=\pm 10^\circ$ (upper mount case)

The changing angle of attack in positive direction shows an asymmetrical behaviour of the vortex pair at $\alpha=5^\circ$ and a complete disappearance of the low pressure spots, which are an indication for the breakdown of the vortex pair.

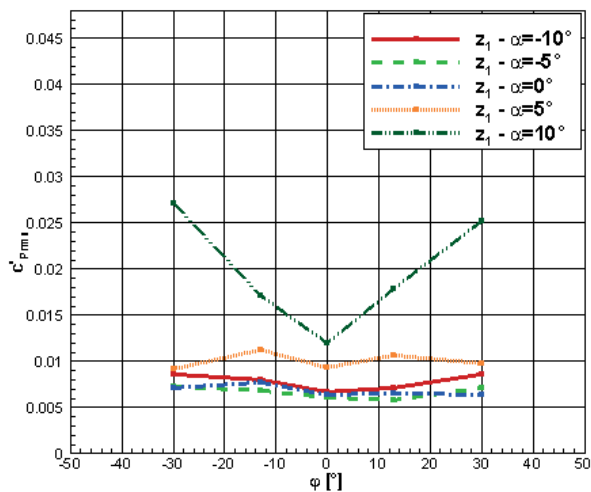


Fig. 15: Root mean square of the pressure coefficient for variation of angle of attack at a slice z_1

The distribution of $C_{p_{rms}}$ for three z-slices with varying angle of attack is shown in Fig. 15 - Fig. 17. At the lowest slice z_1 is no significant change in the fluctuation intensity, besides at $\alpha=10^\circ$, where a

strong rise towards the sidewalls of the fuselage tail can be seen (Fig. 15). This rise can be explained by the movement of the separation zone closer to the sensor points at $\phi=\pm 30^\circ$.

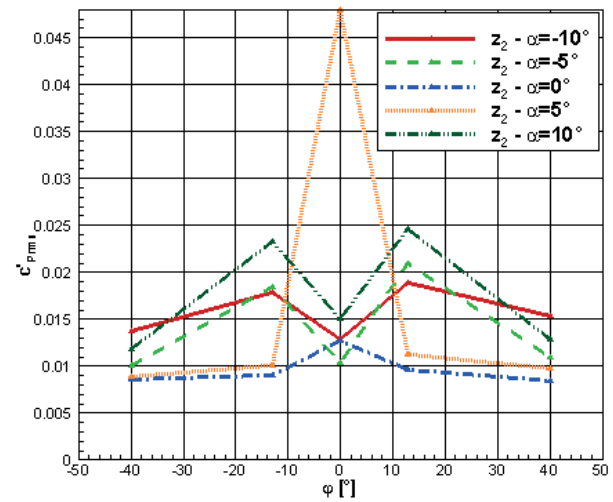


Fig. 16: Root mean square of the pressure coefficient for variation of angle of attack at a slice z_2

At the middle slice z_2 , considerable changes for the alpha-sweep are present (Fig. 16). The baseline case, at $\alpha=0^\circ$, gives one small peak at $\phi=0^\circ$. At $\alpha=5^\circ$ the peak is rising and for $\alpha=10^\circ$ the middle peak fade away and two smaller peaks appear on both sides at $\phi=\pm 13^\circ$. For the negative sweep of α also two peaks can be detected, which remains at the same fluctuation level.

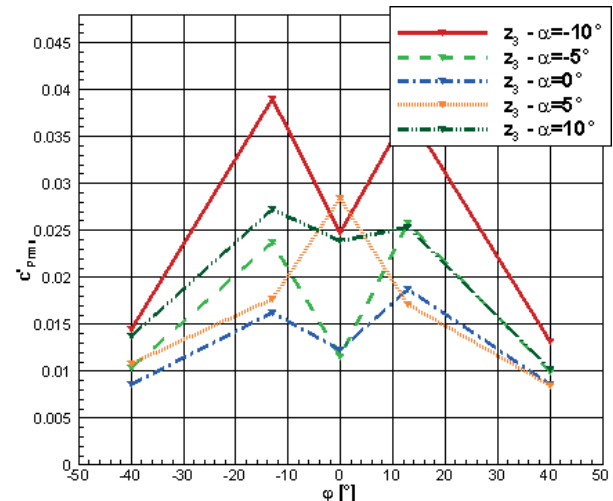


Fig. 17: Root mean square of the pressure coefficient for variation of angle of attack at a slice z_3

Comparing the z_3 -slice with the surface pressure distribution, a trend concerning the effect of the vortex pair on the pressure fluctuations can be

noticed. With negative angle of attack the vortices are getting stronger and the fluctuation of the cores is doing so. At $\alpha=5^\circ$ there is like at z_2 a larger peak which can be assigned to the small spot of rising pressure (Fig. 14d).

4. CONCLUSION

The flow around a helicopter fuselage was investigated experimentally. The focus of the investigations is on the flow phenomena around the lower tail section of the fuselage and in its wake.

The undisturbed flow around the lower tail section of the fuselage shows a strong positive pressure gradient, which gives an indication of flow separation. Two spots of low pressure in this area on the surface showing the generation of a counter rotating vortex pair, which also can be seen in the flow field, measured behind the fuselage. The vortex pair has a higher level of turbulence in its cores, which become noticeable on the surface by pressure fluctuations, as well as in the wake are by velocity fluctuations.

The influence of the model mount on the flow around the lower fuselage tail was shown. Considering the mean flow, the flow strongly affected by the lower cylindrical strut disturbs the generation of a vortex pair on the surface of the fuselage tail. This reduces the strength of the vortices upstream in the wake.

The variation of angle of attack shows a change in the surface pressure distribution, which indicates a shift in the generation of the vortex pair. For negative angle of attacks the amplification of the vortex strength and the fluctuation intensity of the surface pressure are detected. For positive angles of attack a destabilization of the vortex pair can be seen.

5. OUTLOOK

Also the effects caused by the rotorhub, especially depending on the angle of attack, on the surface pressure are not known. Further analyses with a rotating rotorhub will be performed to address this issue.

ACKNOWLEDGMENTS

This research is funded by the German aerospace collaborative project SHANEL-L with grant number 20A0603C. The authors are indebted to Eurocopter Deutschland GmbH.

REFERENCES

1. T. Cebeci, W. Su, The birth of open separation on a prolate spheroid, *Comp. Fluid Dyn.*, 1994, Vol. 1, p.283-307.
2. C. J. Chesnakas, R. L. Simpson, Full three-dimensional measurements of the cross-flow separation of a 6:1 prolate spheroid, *Experiments in Fluids* 17, 1994, p. 68-74.
3. V. Glaze, M. Costes, H. Frhr. von Geyr, N. Kroll, P. Renzoni, M. Amato, A. Kokkalis, L. Mottura, C. Serr, E. Larrey, A. Filippone, A. Fischer, Helicopter Fuselage Drag Prediction: State of the art in Europe, *AIAA Paper* 2001-0999, Jan. 2001.
4. A. Filipone, J. A. Michelsen, Aerodynamic Drag Prediction of Helicopter Fuselage, *Journal of Aircraft*, Vol. 38, No. 2, March-April 2001, p. 326 - 333.
5. F. Le Chuiton, A. D' Alascio, G. Barakos, R. Steijl, D. Schwamborn, H. Lüdeke, Computation of the Helicopter Fuselage Wake with the SST, SAS, DES and XLES Models, *Notes on Numerical Fluid Mechanics and Multidisciplinary Design*, Vol. 97, 2008.
6. F. Vogel, C. Breitsamter, N. A. Adams, Aerodynamic Analysis of a Helicopter Fuselage, *STAB Symposium*, 2008.
7. F. Vogel, C. Breitsamter, N. A. Adams, Aerodynamic investigations on a helicopter fuselage with rotor hub, *34th European Rotorcraft Forum*, 2008.
8. C. Breitsamter, Airbrake induced fin buffet loads on fighter aircraft, *25th International Congress of the Aeronautical sciences*, 2006.